Long-term micro-structure and cerebral blood flow changes in patients recovered from COVID-19 without neurological manifestations

Yuanyuan Qin, … , Jie Wang, Wenzhen Zhu

Clinical Medicine   In-Press Preview   COVID-19   Neuroscience

Graphical abstract

Find the latest version:

https://jci.me/147329/pdf

Long-term micro-structure and cerebral blood flow changes in patients recovered from COVID-19 without neurological manifestations

Subtitle: Variations of brain in recovered COVID-19 patients

Yuanyuan Qin[#1], MD, PhD; Jinfeng Wu[#2], PhD; Tao Chen[#3], MD, PhD; Jia Li[1], MD, PhD; Guiling Zhang[1], Di Wu[1], Yiran Zhou[1], Ning Zheng[2], PhD; Aoling Cai[2], Qin Ning[3], MD, PhD; Anne Manyande[4], PhD; Fuqiang Xu[2, 5], PhD; Jie Wang[*2, 5], PhD; Wenzhen Zhu[*1], MD, PhD

[1] Department of radiology, Tongji Hospital, Tongji Medical College, Huazhong University of Science and Technology; Wuhan, Hubei 430071, P.R. China;

[2] State Key Laboratory of Magnetic Resonance and Atomic and Molecular Physics, Key Laboratory of Magnetic Resonance in Biological Systems, Innovation Academy for Precision Measurement Science and Technology, Chinese Academy of Sciences, Wuhan, Hubei 430071, P.R. China;

[3] Institute and Department of Infectious Disease, Tongji Hospital, Tongji Medical College, Huazhong University of Science and Technology, Wuhan, Hubei 430071, P.R. China;

[4] School of Human and Social Sciences, University of West London, Middlesex, TW89GA, UK;

[5] University of Chinese Academy of Sciences, Beijing 100049, China;

[#]These authors contributed equally to this work.

[*]Co-corresponding to: Jie Wang and Wenzhen Zhu

Jie Wang, PhD

Tel: 86-27-87197653; Email: jie.wang@apm.ac.cn.

Mailing address: Innovation Academy for Precision Measurement Science and Technology, Chinese Academy of Sciences, Wuhan, Hubei 430071, P.R. China;

Wenzhen Zhu, MD, PhD

Tel and Fax: +86-27-83663258; Email: zhuwenzhen8612@163.com

Mailing address: Department of radiology, Tongji Hospital, Tongji Medical College, Huazhong University of Science and Technology, 1095 Jiefang Avenue, Wuhan, 430030, PR China.

Abstract

The coronavirus disease 2019 (COVID-19) rapidly progressed to a global pandemic. Although patients totally recover from COVID-19 pneumonia, long-term effects on the brain still need to be explored. Here, two subtypes (mild type-MG and severe type-SG) with no specific neurological manifestations at the acute stage and no obvious lesions on the conventional MRI three months after discharge were recruited. Changes in gray matter morphometry, cerebral blood flow (CBF) and white matter (WM) microstructure were investigated using MRI. The relationship between brain imaging measurements and inflammation markers were further analyzed. Compared with healthy controls, the decrease in cortical thickness/CBF, and the changes in WM microstructure were observed to be more severe in the SG than MG, especially in the frontal and limbic systems. Furthermore, changes in brain microstructure, CBF and tracts parameters were significantly correlated with inflammatory markers. The indirect injury related to inflammatory storm may damage the brain, that led to these interesting observations. There are also other likely potential causes, such as hypoxemia and dysfunction of vascular endothelium, et al. The abnormalities in these brain areas need to be monitored in the process of complete recovery, which could help clinicians to understand the potential neurological sequelae of COVID-19.

Key words: COVID-19; Brain MRI; Recovered patients; Inflammatory markers; Cortical thickness; Cerebral blood flow; microstructure; gray matter; white matter; subcortical nuclei

Introduction

The highly infectious Coronavirus Disease 2019 (COVID-19), caused by Severe Acute Respiratory Syndrome Coronavirus 2 (SARS-CoV-2) rapidly progressed to a global pandemic and unleashed widespread concern around the world in 2020. To date, it has infected more than 85 million people and killed over 1.8 million worldwide (Data from World Health Organization, WHO, December 31st, 2020). The prominent symptoms of COVID-19 are in the respiratory system, however, growing evidence indicates that the SARS-CoV-2 not only attacks the lungs, kidneys and heart, but also affects the central nervous system (CNS) at the early stage of infection (1, 2). COVID-19 associated neurological manifestations such as encephalitis (3, 4), acute necrotizing encephalopathy (ANE)(5), demyelination (6), cerebrovascular disease (1, 7), Guillain-Barre syndrome (GBS) and its variants(8, 9) have been reported. The underlying mechanisms are potentially related to direct virus infection of the CNS, virus-induced hyperinflammatory and hypercoagulable states and post-infectious immune mediated processes (2, 10). However, previous studies are based on retrospective hospitalized data and focus on the immediate effect of COVID-19, leaving the long-term impact on the brain still unknown (11). The clinical spectrum of COVID-19 ranges from mild, severe to critically ill according to WHO guidelines (12). Critically ill patients, experiencing more severe hypoxia state and inflammatory storm, often have more severe nervous system injury and systemic complications (13). Most patients with mild and severe types usually have no specific neurological symptoms at the acute stage and relatively better clinical outcome (12). Although patients were totally recovered from COVID-19 pneumonia, whether the potential damage to the brain exists or not remains unknown. Thus, the long-term impact on the brain of those patients without any specific neurological manifestations needs to be further investigated, which could yield better understanding of the ongoing neurological and psychological effects and generate clinical guidance toward complete recovery.

In the current study, we aimed to explore the neurological alterations after long-term recovery in recovered COVID-19 patients with no specific neurological manifestations at the acute stage and three months' follow up. The patients diagnosed as mild and severe types of COVID-19 infection according to WHO guidelines and had no specific neurological manifestations during hospitalization were enrolled and followed up for 3 months. The potential changes in brain microstructure and cerebral blood flow (CBF) were investigated and compared with age- and sex-matched healthy controls using quantitative

1   MRI and state-of-the-art post-processing protocols.

2

3   **Results**

4   All patients were enrolled according to the study design in **Figure 1**. Briefly, the participating

5   patients were divided into the mild group (MG) and severe group (SG) according to WHO guidelines.

6   There were no specific neurological manifestations at the acute stage. The inflammatory markers and

7   other demographics and behavioral measures were applied during hospitalization when patients were

8   sick. After three months' recovery, multiple model MRI methods were utilized to investigate changes in

9   the brain structure and blood flow.

10   **Demographics and behavioral measures**

11   As shown in **Table 1**, fifty-one patients recovered from COVID-19 were recruited, including 19

12   mild type (MG) and 32 severe type (SG) patients. Results of the mean hematocrit (Hct) value showed no

13   significant difference between the MG and SG (p=0.835). For males only, the Hct value showed no

14   significant difference between the MG and SG (P=0.923); and the results were also similar for females

15   (P=0.553). This could reduce the Hct effect on CBF and reflect more on the impact of the disease in each

16   group. For inflammatory markers, we found significant elevation of C-reactive protein (CRP) ($p < 0.001$),

17   procalcitonin (PCT) ($p = 0.001$) and interleukin-6 (IL-6) ($p = 0.041$) in the SG compared to the MG. All

18   patients recovered from COVID-19 pneumonia were diagnosed and hospitalized in March, 2020.

19   According to their medical history, all patients showed no specific neurological symptoms during

20   hospitalization, except for coughing, fever, dyspnea, diarrhea, headache, fatigue, myalgia and chest

21   tightness during the SARS-CoV-2 infection. All patients exhibited lesion absorption of the lungs.

22   However, compared to the MG, the SG had more sequelae in the lungs, such as fiber strands and

23   bronchiectasis. **Supplementary Figure S1** illustrates two patients with mild (A-B) and severe types (C-

24   D) of COVID-19 at baseline and three months after discharge. To avoid cross infection, the brain MRI

25   scans were not performed during hospitalization in March, but followed up in late June and early July,

26   which is about three months after discharge. All patients showed no obvious lesions on the conventional

27   MRI. The mean duration from discharge to MRI scanning was 101.21±12.24 days. Another 31 age-, sex-

28   and education-matched non-COVID-19 volunteers were enrolled to the normal control (NC) group.

29

Cortical thickness and subcortical volume comparisons

Compared to the NC, the SG showed significantly (voxel-wise permutation test, p < 0.05) reduced cortical thickness in the left insula (**Figure 2A**, cluster volume (CV): 1742 mm^3, peak MNI coordinates (MNI): -52 -14 12, peak t value (t): 5.4172), left hippocampus (CV: 327 mm^3, MNI: -25 -11 -12, t: 4.178) and left superior temporal gyrus (CV: 366 mm^3, MNI: -40 -35 11, t: 5.2035). No significant differences were observed between the NC and the MG, or between the MG and SG. Correlational analysis further revealed that the cortical thickness of the left hippocampus was negatively correlated with the PCT in the SG (**Figure 2B**).

In subcortical nuclei comparisons, fourteen nuclei volumes were obtained from preprocessing. Namely, the left caudate, right caudate, left putamen, right putamen, left thalamus, right thalamus, left globus pallidus, right globus pallidus, left hippocampus, right hippocampus, left amygdala, right amygdala, left accumbens and right accumbens. For group comparisons, the SG tended to have significantly reduced volumes of the left putamen (, $p = 0.0202$), left thalamus ($p = 0.0370$) and right thalamus ($p = 0.0084$) compared with the NC (**Figure 2C**). The SG was also found to show significantly decreased volumes of the left caudate (, $p = 0.0368$) and left putamen ($p = 0.0284$) than the MG (**Figure 2D**).

CBF comparison

For the SG, CBF values were generally and significantly (voxel-wise permutation test, $p < 0.05$) lower compared with the NC across the gray matter cortex and the peak value was observed in the left insula (**Figure 3A**, MNI: -43 -6 1, t: 6.0816). Further, the peak region insula was manually extracted to conduct the correlational analysis with the level of inflammatory markers. Compared with the MG (**Figure 3B**), the SG exhibited significantly lower CBF values in the bilateral superior medial frontal gyrus (CV: 3417 mm^3, MNI: 1 51 24, t: 5.6017), left insula (CV: 2650 mm^3, MNI: -43 -11 -9, t: 5.3929) and right insula (CV: 381 mm^3, MNI: 43 -15 2, t: 5.377). However, there were no significant differences between the NC and the MG. Correlational results showed that the mean CBF of the left insula in the SG was positively correlated with the level of PCT (**Figure 3C**).

For subcortical nuclei CBF alterations, compared with the NC, the SG exhibited significantly reduced CBF values in the left caudate ($p = 0.0460$), right caudate ($p = 0.0140$), left putamen ($p = 0.0344$),

right putamen ($p = 0.0048$), right globus pallidus ($p = 0.0106$), right hippocampus ($p = 0.0166$), right

amygdala ($p = 0.0160$) and right accumbens ($p = 0.0194$) (**Figure 3D**). Compared with the MG, the SG

showed lower CBF values in the left caudate ($p = 0.0346$), right caudate ($p = 0.0162$), right globus

pallidus ($p = 0.0208$) and right amygdala ($p = 0.0258$) (**Figure 3E**). There were no significant differences

observed between NC and MG.

White matter XTRACT analysis

For a specific tract estimated from a given subject, the shape and position of that tract differed

slightly, and it was inappropriate to conduct the spatially corresponding voxel-wise comparison. For a

given tract, XTRACT yielded multiple post-analysis statistics, three meaningful statistics are exhibited,

i.e. volume, length and fractional anisotropy (FA). Specifically, the volume is a voxel-wise statistic,

every voxel that met the threshold of the estimation of probabilistic diffusion tractography was taken into

account and the total voxel-wise trajectory size was considered the volume. The volume suggests the

most accurate and sensitive statistic in a given tract and was taken as the optimal quantitative statistic.

The statistic length follows the same logic, but due to the slightly different shape of a given trajectory,

the length was not considered as the optimal statistic. FA is a rough tract-wise indicator, revealing only

vague and suggestive information of that specific tract. The significant comparisons between groups are

marked and exhibited in **Supplementary Table S1**. We found widespread decrease in volume, length

and mean FA values in association, commissural, projection and limbic fiber bundles in the MG and SG

when compared with the NC.

Compared to the NC, the MG showed 17 tracts changes in three different measures (Volume: 7;

length:8; FA:2) (**Supplementary Table S1**). For parameter volume, the MG had overall lower values in

the left Acoustic Radiation (AR) ($p = 0.0076$), right Anterior Thalamic Radiation (ATR) ($p = 0.0264$),

left Cingulum Bundle: Dorsal (CBD) ($p = 0.0410$), right Frontal Aslant Tract (FAT) ($p = 0.0464$),

Forceps Minor (FMI) ($p = 0.0410$), left Inferior Longitudinal Fasciculus (ILF) ($p = 0.0084$), right ILF ($p = 0.0094$) (**Figure 4A**). Using these 17 different tracts measures, the first principal component (PC1)

was obtained, which represents 35.1% of the total variance of the different parameters. The correlation

analysis indicated that PC1 was only significantly correlated with one of the three inflammatory markers,

namely PCT ($p = 0.0483$, **Figure 4B**). To calculate the contribution of the different tracts, the

correlational analysis between the different parameters and PCT was calculated, which revealed that the volume of the right ATR (**Figure 4C**) and right ILF (**Figure 4D**) were negatively and significantly correlated with the PCT in the MG.

Compared to the NC, the SG showed 33 tracts changes in three different parameters (Volume: 12; length: 5; FA:16) (**Supplementary Table S1**). For parameter volume, the SG showed overall lower values in the right ATR ($p = 0.0134$), left CBD ($p = 0.0076$), right CBD ($p = 0.0312$), left Corticospinal Tract (CST) ($p = 0.0412$), right FAT ($p = 0.0284$), FMI ($p = 0.0130$), left Fornix (FX) ($p = 0.0232$), right Inferior Fronto-Occipital Fasciculus (IFO) ($p = 0.0162$), left ILF ($p = 0.0046$), right ILF ($p = 0.0014$), right Optic Radiation (OR) ($p = 0.0146$) and left Superior Longitudinal Fasciculus II (SLF2) ($p = 0.0206$) (**Figure 5**). Note that the volumes of the right ATR, left CBD, right FAT, FMI, left ILF and right ILF were decreased in the MG and the SG compared to the NC. With these changed tracts (n = 33), PC1 was calculated, which represents 26.1% of the total variance of the parameters. The correlation analysis showed that PC1 was only significantly correlated with IL-6 ($p = 0.0430$, **Figure 6A**). To calculate the contribution of the different white matters, the correlations of different tracts and IL-6 were calculated. Correlational analysis revealed that the volumes of the left CST and the right OR were significantly positively correlated with IL-6; Moreover, the FA on the left of the Middle Longitudinal Fasciculus (MDLF) were also significantly positively correlated with IL-6 (**Figure 6B-6D**).

Discussion

Our findings demonstrated that, the mild and severe type COVID-19 patients with no specific neurological manifestations or obvious lesions on the conventional MRI, although totally recovered from pneumonia, still exhibited brain microstructure changes and decrease in CBF after a three months' follow up. Compared with healthy controls, just a few changes were found in the white matter tract in the mild group, with no significant changes in gray matter and CBF. The decrease in cortical thickness, changes in white matter microstructure and decrease in regional CBF were much more profound and extensive in the severe group than in the mild group, especially in the frontal and limbic systems. Furthermore, the brain microstructure changes and CBF decrease were highly correlated with the level of inflammatory markers in the severe group. The abnormalities in these brain areas could help clinicians to understand the potential neurological sequelae of COVID-19.

Cortical abnormality

Brain integrity appears to be vulnerable to systemic inflammation during critical illness. In our study, the SG had significantly lower cortical thickness in the left insula, left hippocampus and left superior temporal gyrus compared with the NC but no significant differences were seen between the MG and the NC. A study by Lindlau. et al suggested that high levels of the PCT and IL-6 in the blood serum of critically ill patients are associated with a higher likelihood of hippocampal atrophy (14) six months after discharge from intensive care unit. Similarly, we also found that atrophy of the hippocampus was negatively correlated with PCT in recovered COVID-19 patients. The hippocampus plays a key role in both memory formation and spatial navigation, and has the capacity to support flexible cognition and behavior (15). The hippocampal volume has also been shown to be sensitive to stress severity (16). In our study, COVID-19 infection was a very stressful event for patients, and even for their family members. Thus, hippocampal impairment could partly be attributed to the influence of a stressful event and partly to hypoxia or other processes. A recent retrospective study on brain MRI findings in acute SARS-CoV-2 infection indicated that signal abnormalities in the medial temporal lobe appeared more frequently in patients with severe COVID-19 (17), such as in the case of herpesvirus encephalitis or autoimmune limbic encephalitis. With no acute neurological manifestations, the recovered severe type patients still showed gray matter atrophy in the left insula, left hippocampus and left superior temporal gyrus in this study, which are all important components of the limbic system. Our study indicates a possible vulnerability of the limbic system for COVID-19 infection, which may be partly aligned with the angiotensin converting enzyme 2 (ACE-2) rich region in the brain.

In the current study, the CBF in the SG was generally lower across the bilateral frontal and temporal cortex than in the NC, with the lowest region in the left insula. In line with a previous study (18), the SG with bilateral frontal-temporal involvement may suffer much more severe hypoxic state, which may be the underlying pathogenesis. Clinically, the breakdown or dysfunction of the blood brain barrier can accompany hypoxia, which results in such an overall cortical blood flow decrease (19). Group comparison between the MG and the SG showed that significant abnormal blood flow appeared in the bilateral insula and superior medial frontal gyrus.

In the cortical analyses of thickness and blood flow, the insula constantly exhibited abnormality in group comparisons. A previous study showed that the insular cortex is hidden under dense arterial and venous

blood vessels (20), making it easily influenced by pneumonia introduced hypoxia. So, the deformation and disfunction of the insula in COVID-19 patients was obvious. Sufficient evidence has demonstrated that the insula subserves a wide variety of functions in humans ranging from sensory and affective processing to high-level cognition(20), while the precise functional impact of insular abnormality remains unclear. There is also another alternative explanation. For gray matter thickness, we firstly used 3D-T1 images to segment the whole brain in to gray matter, white matter and CSF, then the T1 values were used to estimate the thickness of the gray matter. If the COVID-19 infection alters the T1 of gray matter, which is possible given the proposed changes in tissue microstructure, then the altered T1 values could make it look like the thickness of the gray matter has changed. Furthermore, another interesting finding is that the CBF in the left insula in the SG was positively but not negatively associated with the PCT. The positive correlation possibly implies that the more severe the inflammation is, the more severe the damage is in the insula when patients are hospitalized. As the MRI imaging was conducted 3 months after discharge, we speculated that the more severe the damage is, the faster the recovery would be for severe type patients. This is a very preliminary study and further longitudinal follow up studies are needed to confirm this speculation.

Subcortical abnormality

Subcortical nuclei analysis of the volume and CBF also revealed a decreasing pattern that is consistent with cortical thickness analysis, suggesting that the impact of COVID-19 is brain-wide. The bilateral thalamus and left putamen exhibited decreased volume in the SG relative to the NC. However, there were no subcortical nuclei volume differences between the NC and the MG, whereas the MG-SG comparison showed abnormality in the left putamen and caudate. The bilateral thalamus is a susceptible target of ANE related to late immune demyelination in COVID-19 (5) and also brain regions sensitive to hypoxemia. The caudate and putamen as parts of the human striatum are distinguished by a marked heterogeneity in functional, anatomical, and neurochemical patterns (21). For CBF comparisons, the SG showed more widespread CBF decrease in the subcortical nuclei mainly located in the striatum and amygdala compared to the MG. These results suggest that COVID-19 severity may elicit different influence even damage to the critical subcortical nuclei. Follow-up functional analysis will be conducted to address the precise functional abnormality of subcortical nuclei.

For the subcortical white matter tracts analysis, we adopted a new robust and reproducible tool XTRACT, which allows reconstruction of white matter tracts in a consistent manner across subjects, whilst respecting the underlying anatomical variation and individual differences (22). We found widespread decrease in volume, length and the mean FA value in association, commissural, projection, and limbic fiber bundles in the MG and SG when compared with the NC. In the MG and SG, the volume of several tracts which belong to four different fiber bundles decreased when compared to the NC, with the SG showing more fiber impairment relative to the MG. The significant tracts, right ATR, left CBD, right FAT, FMI, left ILF, right ILF, were overlapped in the NC-MG and NC-SG comparisons, while, there were no significant differences between the MG and SG, suggesting that COVID-19 impaired the white matter in both the MG and SG to a different extent.

For correlational analyses, in the MG, the volume decreases in the right ATR and the right ILF were significantly associated with PCT elevation during hospitalization, indicating that the more severe the disease, the lower the volume of the tracts. This indicates that a high level of inflammatory markers during hospitalization were associated with a high likelihood of volume loss in recovered COVID-19 patients, especially in frontal and limbic systems. This is consistent with the cortical thickness alterations in our study.

There is also another interesting finding in the SG. The volumes of the left CST and right OR, the mean FA value of the left MDLF showed positive correlations with the level of IL-6. Thus, we hypothesized that the white matter could be seriously damaged due to COVID-19 infection, especially for the severe patients. The volumes and mean FA value of the white matter tracts could be significantly decreased in several brain regions. However, it gradually recovered after patients were cured. The more severe the COVID-19 condition, the more changes in white matter occurred in several brain regions. Thus, we speculated that the brain injury in the SG was more severe than that in the MG during hospitalization, as some tracts' recovery rate in the SG was more rapid than in the MG after three months' recovery. This is somehow similar to the structural remodeling observed in arrhythmia manifestations of COVID-19 infection (23). Regardless of whether the correlation was positive or negative, the white matter microstructure changes were related to inflammation to some extent. More importantly, in the severe type group, the connections between brain imaging measurements and inflammatory markers are

more obvious than in the mild type group. However, the underlying mechanisms remain unclear, and further quantitative analysis is needed.

Potential mechanism of brain injury

Although totally recovered from pneumonia symptoms, the recovered COVID-19 patients still exhibited brain microstructure and CBF changes three months after recovery. There should be several possible pathogenic mechanisms to explain the influence of COVID-19 on cerebral damage, such as direct viral encephalitis, peripheral organ dysfunction (such as lung, liver, kidney), cerebrovascular changes and systemic inflammation (24). The dissemination of COVID-19 in the systemic circulation or across the cribriform plate of the ethmoid bone can lead to cerebral involvement which has been reported in the past for SARS-CoV affected patients (25). This is the direct mechanism of COVID-19 related brain damage during the acute stage reported in previous studies. In our three months' follow up study, patients had no specific or acute neurological problems during the acute period of the disease and the major difference between the MG and the SG was that the SG experienced a more severe hypoxic state and inflammatory storm. Correspondingly, the brain imaging measurements in the SG were much more extensive than in the MG in which just a few changes were found in the white matter tract. The changes in the brain, such as cerebral volumes, cerebral blood flow and white matter tracts, were highly correlated with inflammatory factors in the severe group. Thus, we assumed that the main underlying mechanism could be related to indirect injury due to an inflammatory storm induced by the immune response (26) or hypoxia. Furthermore, neuropathologic features of autopsied COVID-19 also showed various hypoxia-injury in the brain, such as cell abundant enlarged perivascular spaces, with no signs of encephalitis or meningitis (27, 28). Neurochemical measurements also showed that COVID-19 patients with different severity states had varying degrees of neuronal injury and glial activation, supporting that indirect injury is the main mechanism and not the direct invasion of the virus (12). On the other hand, hypercoagulability and microembolization of the vascular endothelium may also be implicated, as evidenced by the hypoperfusion on arterial spin label (ASL) across the gray matter cortex in severe type. In our limited cases, a small number of severe type patients also had kidney or heart damage, leading us to believe that the multi-organ injury could be another possible mechanism. Taken together, all those observations point to the indirect injury mechanism in the brain during long-term recovery.

Limitations

There are several limitations in this study. First, the sample size is small, we should aim to increase the sample size in a further follow up study. Second, patients had no specific neurological manifestation and so, to avoid cross-infection, the head MRI was not performed during the acute phase. Third, a follow-up study should be conducted to see whether brain anatomical and functional changes progress or regress.

Conclusion

In this study, gray matter atrophy, widespread CBF reduction and white matter microstructure changes detected by the quantitative MRI technique were found in patients recovered from COVID-19 pneumonia, providing new evidence to the neurological damage of COVID-19 on long-term recovery. The abnormalities in these brain areas should be monitored in the process of complete recovery, which would help clinicians to understand the potential neurological sequelae of COVID-19.

Materials and Methods

Participants

All patients recovered from COVID-19 pneumonia were recruited from the Department of Infectious Disease in Tongji Hospital, with the inclusion criteria as follows: 1) 50-70 years old; 2) diagnosed as mild or severe type of COVID-19 according to WHO interim guidance during hospitalization and did not stay in intensive care unit; 3) had no specific neurological manifestations during the acute stage, such as smell/vision/hearing/taste/memory loss, seizures, impaired mobility; 4) the follow up period is about 3 months after discharge from hospital, with no specific neurological manifestations and no obvious lesion on the conventional MRI; 5) no history of head trauma, stroke, brain tumors, metabolic disturbance, or epilepsy; 6) blood sample was available to get the hematocrit value before the MRI scan. The clinical information of COVID-19 patients was obtained from their hospital records including clinical type, inflammatory markers such as CRP, PCT and IL-6. Age-, sex- and education-matched non-COVID-19 healthy volunteers were recruited from the local community, excluding previous history of head trauma, stroke, brain tumors, metabolic disturbance and epilepsy. Also, polycythemia and anemia were all excluded to ensure the accuracy of CBF calculation. All participants were fully informed about the

purpose of the study and agreed to take the head MRI and chest CT scan and completed questionnaires including age, sex, education years, handedness and underlying diseases on the same day.

Blood test

The levels of PCT and IL-6 were detected using an automatic Biochemical analyzer (Roche Cobas e602, Switzerland). The levels of CRP (IATRON) were detected using a biochemical analyzer (Roche Cobas 8000, Switzerland). The hematocrit (routine blood test) were performed using Sysmex Automated Hematology Analyzer (XS 500i, Japan).

MRI scan

The MRI scan was performed using a 3.0 T MR scanner (Discovery MR750; GE Healthcare, Milwaukee, WI, USA) with a 32-channel head array coil. The protocol included conventional MRI, structural 3-Dimensional T1-weighted Images (3D-T1WI), high resolution diffusion tensor imaging (DTI) and 3D pseudo-continuous arterial spin labeling (3D-pcASL). Foam padding and ear plugs were used to reduce head motion and scanner noise.

The conventional MRI protocol included axial T2-FLAIR sequence with TR/TE/TI =8400/165/2100ms, matrix size =256 × 256, FOV = 240 ×240 mm^2, slice thickness/gap = 5/1.5mm, number of slices =16.

3D-T1WI was acquired using brain volume (BRAVO) sequence with TR/TE/TI=7.1/2.7/450ms, flip angle = 12°, matrix=256 × 256, FOV= 240 × 280 mm^2, number of averages= 1, slice thickness = 1mm, number of slices=184.

DTI was obtained using a single-shot diffusion-weighted echo-planar imaging (EPI) sequence in the axial plane with TR/TE= 8500/60.4 ms, matrix =128×128, FOV= 256×256mm, slice thickness/gap =2/0mm, b value =1000s/mm^2 along 64 directions, 10 b$_0$ images, number of slices=70.

3D-pcASL was acquired using an interleaved 3D stack of spirals fast spin echo (FSE) sequence with a high-level background suppression to cover the whole brain. The detailed parameters were as follows: TR/TE=4788/14.6 ms, post label delay (PLD)= 1525 ms, number of averages= 3, bandwidth=62.5 kHz, readout of 8 arms × 1024 samples, FOV = 240 × 240mm, slice thickness/gap=4/0mm, number of slices =34. The labeling duration is 1500msec and the resolution is 4

× 4× 4mm.

To ensure the robustness of our analyses, image quality control was strictly performed from acquisition to preprocessing. The quality of the signal fidelity, brain extraction and registration in each stage on every image were plotted and visually checked. Subjects with signal loss, artefacts, poor registration and large head motion were excluded from further analysis. In the current study, no subjects were excluded due to poor quality image and registration. Two healthy volunteers were excluded due to signal loss in the cerebellum of raw images.

MRI data preprocessing

Cortical thickness evaluation

To obtain accurate native space skull-stripped brain masks, segmentations and MNI space warped subcortical nuclei volumes, 3D-T1WI were uploaded to the online anatomical segmentation pipeline volBrain (29). According to our prior experience and visual check, the machine-learning based volBrain pipeline produced clear-cut grey matter, white matter, cerebrospinal fluid (CSF), subcortical nuclei segmentations and the results were much better than other algorithms such as BET in FSL (FMRIB Software Library)(30), FreeSurfer (31) and ANTs (Advanced Normalization Tools, http://stnava.github.io/ANTs/). The native brain masks and subcortical segmentations were used in the following analyses.

The cortical thickness evaluation was conducted using ANTs (32). The automated, volume-based ANTs cortical thickness pipeline comprised of well-vetted components such as SyN (image registration), N4 (bias correction), Atropos (n-tissue segmentation) and DiReCT (cortical thickness estimation). The ANTs cortical thickness estimation workflow is illustrated in **Figure 7**. The steps were as follows: (1) Initial N4 bias correction on T1 images; (2) Brain extraction using a segmentation/template-based strategy, i.e. 6 segments priors (cerebrospinal fluid prior, gray matter prior, white matter prior, subcortical nuclei prior, cerebellum prior, brainstem prior) were specified before; (3) Alternation between prior-based segmentation and "pure tissue" posterior probability weighted bias correction using Atropos and N4; (4) DiReCT-based cortical thickness estimation; (5) Normalize to MNI (Montreal Neurological Institute) 1mm resolution template.

1   ANTs cortical thickness evaluation was shown to have a higher predictive performance than

2 FreeSurfer measures (32). Notice that the ANTs only yielded the cortical thickness results and subcortical

3 nuclei volumes were derived from volBrain. **Figure 7** demonstrates the workflow of ANTs cortical

4 thickness estimation.

5

6 **pcASL preprocessing**

7   All raw pcASL images were transferred to the workstation (Advantage Workstation 4.6; GE

8 Medical Systems) to obtain the native CBF map according to the kinetic model proposed by Alsop and

9 Detre (33). In addition, we included a term for the finite labeling duration and corrected the incomplete

10 recovery of the tissue signal in the reference image due to the saturation performed t_{sat} (2000 msec) before

11 imaging(34). The quantitative CBF maps were based on the following equation:

12
$$CBF = \frac{\lambda}{2\alpha T_{1b}\left(1 - e^{-\frac{\tau}{T_{1b}}}\right)} \frac{(S_{ctrl-}\,S_{lbl})\left(1 - e^{-\frac{t_{sat}}{T_{1g}}}\right)}{S_{ref}} e^{\frac{\omega}{T_{1b}}}$$

13   Where S_{ctrl}, S_{lbl}, S_{ref} is the signal on the control, label and reference image; T_{1b} is the T1 relaxation

14 time of the blood at 3.0T about 1600 msec, T_{1g} represents the T1 relaxation time of the gray matter at

15 3.0T about 1200 msec, t_{sat} is the time of saturation performed before imaging about 2000 msec, α is the

16 labeling efficiency of 0.8, λ is cortex-blood partition coefficient of 0.9, τ is the labeling duration about

17 1500 msec, and ω is the post labeling delay time of 1525 msec.

18   The preprocessed native CBF images were aligned to the T1 images using FLIRT pipeline in FSL

19 tools and then warped into the MNI space using subject-specific ANTs warp fields produced previously.

20 To obtain the subcortical nuclei CBF, the subcortical nuclei masks in the MNI space were obtained from

21 volBrain, then the masks were used to extract the subcortical nuclei CBF.

22

23 **DTI preprocessing**

24   The DTI images were preprocessed using FDT pipeline in the FSL. The steps were as follows:　(1)

25 Eddy current correction was first conducted (EDDY); (2) brain extraction on first B0 image (BET) and

26 then applied the native mask to the rest of the images; (3) fitting of the diffusion tensors on corrected

27 data (DTIFIT); (4) Fitting of the probabilistic diffusion model on corrected data (BEDPOSTX); (5) using

the first B0 image as the reference, linearly registered the B0 image to T1 image (FLIRT); (6) spatial

normalization from T1 to the MNI space (FNIRT); (7) finally, performing a newly-developed pipeline

to automatically extract a set of carefully dissected tracts (**Figure 8A**) in the subject's native space using

probabilistic diffusion tractography(22) .

XTRACT is a new software package with a library of standardized tractography protocols

(BEDPOSTX and PROBTRACKX) devised for the robust automated extraction of white matter (**Figure**

8B). Deriving data from the Human Connectome Project (HCP) and the UK Biobank, white matter

atlases and atlases for tract endpoints on the white-grey matter boundary were obtained. These automated

ROI-based tractography approaches have proven powerful in the extraction of a range of tracts. The

tractography reflects the known anatomy and prior anatomical knowledge used to guide and constrain

curve propagation, reducing the chance of false positives (35, 36).

The algorithm BEDPOSTX stands for Bayesian Estimation of Diffusion Parameters Obtained using

Sampling Techniques. The X stands for modelling crossing fibers within each voxel of the brain.

BEDPOSTX runs Markov Chain Monte Carlo sampling to build up distributions on diffusion parameters

at each voxel. Crucially, BEDPOSTX automatically determines the number of crossing fibers per voxel.

It creates all the files necessary for running probabilistic tractography PROBTRACKX.

PROBTRACKX produces sample tractographies, by starting from some seeds and then iterate

between (1) drawing an orientation from the voxel-wise BEDPOSTX distributions, (2) taking a step in

this direction, and (3) checking for any termination criteria. These sample tractographies can then be

used to build up a histogram of how many tractographies visited each voxel or the number of

tractographies connecting specific brain regions. The probabilistic estimation of multi-fiber tractography

at each voxel offers significant advantages in sensitivity when tracking non-dominant fiber populations

but does not dramatically change tractography results for the dominant pathways.

Statistics

To ensure statistical consistency, all comparisons were conducted using the permutation test (5000

random shuffles of subjects' labels, $p < 0.05$). The statistical analysis on the cortical thickness images

and pcASL CBF images were performed using the permutation test (randomise in FSL) (37) with the

TFCE (threshold-free cluster enhancement).

The statistical comparison of subcortical nuclei volumes, subcortical CBF values and tract statistics were performed using custom code in MATLAB (R2020a, The MathWorks, Inc.). Specifically, for a given nucleus/tract in one group comparison, the difference of the given nucleus/tract between each group was calculated, i.e. the real statistic and then 5000 random shuffles of subjects' labels were performed. We then recalculated the difference in each shuffle iteration to generate a permutation distribution, and finally the upper-threshold is the real statistic at 95 percentage of the permutation distribution (38). 5000 permutations were demonstrated to be robust for generating the null distribution, it yielded no differences when set to 10000 permutations. Due to consideration of the age effect on subcortical nuclei, age was regressed out before the permutation test. However, we found that whether regressed out or not, age had no influence on the results in the permutation test.

To further explore the relationships between the MRI image features and inflammatory biomarkers, we first regressed out the age effect on the resultant significant cortical brain regions, subcortical nuclei volumes, subcortical CBF values and tract volume/length/FA, then the principal component analysis was utilized to reduce the dimensionality of the significant different imaging results. As a common statistical multivariate approach, PCA can generate a new set of variables (principal components-PCs) with minimal loss of information (39). The PCs are generated with a linear combination of the original variables and generate a low-dimensional space which preserves most of the data variance. Then the first component (PC1) was correlated (Pearson correlation) with the inflammatory markers' values, and $P < 0.05$ was considered statistically significant. To explore the contribution of the significant changes in imaging results, the imaging results were further correlated (Pearson correlation) with the values of the upper significant findings related to inflammatory markers. $P < 0.05$ was considered statistically significant. Categorical data were compared using the Fisher exact test, demographic and behavior measures were compared using the student's t-test.

Study approval

This cross-sectional study was approved by the Clinical Institute Ethics Committee of Tongji hospital (Wuhan, China). Written informed consent was obtained from each participant.

Conflict of interest statement

The authors declare that there is no conflict of interest.

References:

1. Mao L, et al. Neurologic Manifestations of Hospitalized Patients With Coronavirus Disease 2019 in Wuhan, China. *JAMA Neurol.* 2020;77:683-690.

2. Pezzini A, Padovani A. Lifting the mask on neurological manifestations of COVID-19. *Nature Reviews Neurology.* 2020;16:636-644.

3. Moriguchi T, et al. A first case of meningitis/encephalitis associated with SARS-Coronavirus-2. *Int J Infect Dis.* 2020;94:55-58.

4. Huang YH, Jiang D, Huang JT. SARS-CoV-2 Detected in Cerebrospinal Fluid by PCR in a Case of COVID-19 Encephalitis. *Brain Behav Immun.* 2020;87:149.

5. Poyiadji N, Shahin G, Noujaim D, Stone M, Patel S, Griffith B. COVID-19-associated Acute Hemorrhagic Necrotizing Encephalopathy: Imaging Features. *Radiology.* 2020;296:E119-E120.

6. Parsons T, Banks S, Bae C, Gelber J, Alahmadi H, Tichauer M. COVID-19-associated acute disseminated encephalomyelitis (ADEM). *J Neurol.* 2020;267:2799-2802.

7. Hernandez-Fernandez F, et al. Cerebrovascular disease in patients with COVID-19: neuroimaging, histological and clinical description. *Brain.* 2020;143:3089-3103.

8. Zhao H, Shen D, Zhou H, Liu J, Chen S. Guillain-Barre syndrome associated with SARS-CoV-2 infection: causality or coincidence? *Lancet Neurol.* 2020;19:383-384.

9. Gutierrez-Ortiz C, Mendez A, Rodrigo-Rey S, San Pedro-Murillo E, Bermejo-Guerrero L, Gordo-Manas R, de Aragon-Gomez F, Benito-Leon J. Miller Fisher Syndrome and polyneuritis cranialis in COVID-19. *Neurology.* 2020;95:e601-e605.

10. Koralnik IJ, Tyler KL. COVID-19: A Global Threat to the Nervous System. *Ann Neurol.* 2020;88:1-11.

11. Enkirch SJ, Traschutz A, Muller A, Widmann CN, Gielen GH, Heneka MT, Jurcoane A, Schild HH, Hattingen E. The ERICA Score: An MR Imaging-based Visual Scoring System for the Assessment of Entorhinal Cortex Atrophy in Alzheimer Disease. *Radiology.* 2018;288:226-333.

12. Kanberg N, Ashton NJ, Andersson LM, Yilmaz A, Lindh M, Nilsson S, Price RW, Blennow K, Zetterberg H, Gisslen M. Neurochemical evidence of astrocytic and neuronal injury commonly found in COVID-19. *Neurology.* 2020;95:e1754-e1759.

13. Xiong W, et al. New onset neurologic events in people with COVID-19 in 3 regions in China. *Neurology.* 2020;95:e1479-e1487.

14. Lindlau A, Widmann CN, Putensen C, Jessen F, Semmler A, Heneka MT. Predictors of hippocampal atrophy in critically ill patients. *Eur J Neurol.* 2015;22:410-415.

15. Bellmund JLS, Gardenfors P, Moser EI, Doeller CF. Navigating cognition: Spatial codes for human thinking. *Science.* 2018;362:eaat6766.

16. Kim EJ, Pellman B, Kim JJ. Stress effects on the hippocampus: a critical review. *Learn Mem.* 2015;22:411-416.

17. Kremer S, et al. Brain MRI Findings in Severe COVID-19: A Retrospective Observational Study. *Radiology.* 2020;297:E242-E251.

18. Helms J, et al. Neurologic Features in Severe SARS-CoV-2 Infection. *N Engl J Med.* 2020;382:2268-2270.

19. Kandemirli SG, et al. Brain MRI Findings in Patients in the Intensive Care Unit with COVID-19 Infection. *Radiology.* 2020;297:E232-E235.

20. Uddin LQ, Nomi JS, Hebert-Seropian B, Ghaziri J, Boucher O. Structure and Function of the Human Insula. *J Clin Neurophysiol.* 2017;34:300-306.

21. Hortnagl H, Pifl C, Hortnagl E, Reiner A, Sperk G. Distinct gradients of various neurotransmitter markers in caudate nucleus and putamen of the human brain. *J Neurochem.* 2020;152:650-662.

22. Warrington S, Bryant KL, Khrapitchev AA, Sallet J, Charquero-Ballester M, Douaud G, Jbabdi S, Mars RB, Sotiropoulos SN. XTRACT - Standardised protocols for automated tractography in the human and macaque brain. *Neuroimage.* 2020;217:116923.

23. Babapoor-Farrokhran S, Rasekhi RT, Gill D, Babapoor S, Amanullah A. Arrhythmia in COVID-19. *SN Compr Clin Med.* In press.

24. Heneka MT, Golenbock D, Latz E, Morgan D, Brown R. Immediate and long-term consequences of COVID-19 infections for the development of neurological disease. *Alzheimers Research & Therapy.* 2020;12:69.

25. Baig AM, Khaleeq A, Ali U, Syeda H. Evidence of the COVID-19 Virus Targeting the CNS:

Tissue Distribution, Host-Virus Interaction, and Proposed Neurotropic Mechanisms. *ACS Chem Neurosci.* 2020;11:995-998.

26. Huang C, et al. Clinical features of patients infected with 2019 novel coronavirus in Wuhan, China. *Lancet.* 2020;395:497-506.

27. Solomon IH, Normandin E, Bhattacharyya S, Mukerji SS, Keller K, Ali AS, Adams G, Hornick JL, Padera RF, Jr., Sabeti P. Neuropathological Features of Covid-19. *N Engl J Med.* 2020;383:989-992.

28. Kantonen J, et al. Neuropathologic features of four autopsied COVID-19 patients. *Brain Pathol.* 2020;30:1012-1016.

29. Manjon JV, Coupe P. volBrain: An Online MRI Brain Volumetry System. *Front Neuroinform.* 2016;10:30.

30. Jenkinson M, Beckmann CF, Behrens TE, Woolrich MW, Smith SM. FSL. *Neuroimage.* 2012;62:782-790.

31. Fischl B. FreeSurfer. *Neuroimage.* 2012;62:774-781.

32. Tustison NJ, et al. Large-scale evaluation of ANTs and FreeSurfer cortical thickness measurements. *Neuroimage.* 2014;99:166-179.

33. Alsop DC, Detre JA. Reduced transit-time sensitivity in noninvasive magnetic resonance imaging of human cerebral blood flow. *J Cereb Blood Flow Metab.* 1996;16:1236-1249.

34. Wu B, Lou X, Wu X, Ma L. Intra- and interscanner reliability and reproducibility of 3D whole-brain pseudo-continuous arterial spin-labeling MR perfusion at 3T. *J Magn Reson Imaging.* 2014;39:402-409.

35. Catani M, Howard RJ, Pajevic S, Jones DK. Virtual in vivo interactive dissection of white matter fasciculi in the human brain. *Neuroimage.* 2002;17:77-94.

36. Wakana S, Jiang H, Nagae-Poetscher LM, van Zijl PC, Mori S. Fiber tract-based atlas of human white matter anatomy. *Radiology.* 2004;230:77-87.

37. Winkler AM, Ridgway GR, Webster MA, Smith SM, Nichols TE. Permutation inference for the general linear model. *Neuroimage.* 2014;92:381-397.

38. Nichols TE, Holmes AP. Nonparametric permutation tests for functional neuroimaging: a primer with examples. *Hum Brain Mapp.* 2002;15:1-25.

39. Higgins V, Hooshmand S, Adeli K. Principal component and correlation analysis of biochemical and endocrine markers in a healthy pediatric population (CALIPER). *Clinical Biochemistry.* 2019;66:29-36.

Figure 1. Flow diagram of the experimental design. MG = mild group, SG = severe group, CRP = C-reactive protein, IL-6 = interleukin-6, PCT = procalcitonin, MRI = magnetic resonance imaging, BRAVO = brain volume, pcASL = pseudo-continuous arterial spin labeling, DTI = diffusion tensor imaging, NC = normal control.

Figure 2. Cortical and subcortical morphology analyses of the recovered COVID-19 patients (sample size NC = 31, MG = 19, SG = 32; permutation test, $p < 0.05$). (A) Significant cortical thickness differences between the NC and SG. (B) Significant negative correlations between the left hippocampus thickness and inflammatory marker PCT values in the SG ($r = -0.38$, $p = 0.0420$). Results of subcortical nuclei volume comparisons between the NC and SG (C-Left: NC; Right: SG), MG and SG (D-Left: MG; Right: SG), as exhibited in the violin plot. *Note*: The trunk size shows the probability density of the data at different values, the bigger the trunk, the denser the values appeared at that level. The notch indicates the 25% median and 75% interquartile range. The mean value of the group is shown by solid line. The bigger the standard deviation, the thinner the violin plot. The brain slices of subcortical nuclei were extracted from a subject. Left violin plots indicate the NC/MG, right violin plots indicate the SG. STG: superior temporal gyrus.

Figure 3. Significant differences in cortical and subcortical CBF between groups (permutation test, $p < 0.05$): (A) NC (n=31) and SG (n=32); (B) MG (n=19) and SG (n=32). (C) Significant positive correlation between the left insula CBF and inflammatory marker PCT values in the SG ($r = 0.3738$, $p = 0.0458$). Results of the comparisons of the CBF in the subcortical nuclei between groups: (D) NC and SG; (E) MG and SG. Note: SMFG: superior medial frontal gyrus. Left of the brain images is actually the right side of the brain. Accu: accumbens; Amy: amygdala; Cau: caudate; GP: globus pallidus; Hippo: hippocampus; Pu: putamen; L = left; R = right. Left violin plots indicate NC/MG, right violin plots indicate SG.

Figure 4. Significant difference in tracts' volume between the NC (n=31) and MG (n=19) (permutation test, $p < 0.05$). The brain slice of a specific tract from HCP population is displayed in the right corner. For standardization, these tracts were extracted from the HCP population instead of the subjects' specific tracts. The principal component 1 (B), volumes of the right

ATR (C) and right ILF (D) showed a significant correlation with the PCT level in the MG (p < 0.05). Note: Left violin plots indicate the NC, right violin plots indicate the MG.

Figure 5. Significant difference of the tracts' volume between the NC (n=31) and the SG (n=32), as shown in violin plots (permutation test, p < 0.05). The brain slice of a specific tract from the HCP population is displayed in the right corner. For standardization, these tracts were extracted from the HCP population instead of the subjects' specific tracts. Note: Left violin plots indicate the NC, right violin plots indicate the SG.

Figure 6. Correlations between the significantly different tracts and inflammatory markers in the SG (n=32) (p < 0.05). Correlations between the principal component 1(A), FA of left MDLF (B), volume of the left CST(C), volume of the right OR (D) and IL-6 respectively. Note: L = left; R = right.

Figure 7. Workflow of ANTs cortical thickness estimation. ANTs cortical thickness pipeline yielded clear-cut brain extraction and 6 tissues segmentation, as well as nearly perfect estimation of thickness in the native space and accurate warping into the MNI space.

Figure 8. Illustration of the method of XTRACT automated tractography. (A): Diagram of the steps for the XTRACT automated tractography, with an example of the left inferior fronto-occipital fasciculus (IFO). Tractography protocol masks were defined in standard space (FSL_HCP1065 FA atlas, derived from the HCP dataset) with seed (start point, blue), exclusion (rejection, black), target (destination, green) and stop (termination, red) masks. The native and standard tractography maps were extracted from a subject from the current sample. (B): Illustration of the projections of the HCP population tract atlases. Association fiber bundles: Arcuate Fasciculus (AF), Frontal Aslant Tract (FAT), Inferior Longitudinal Fasciculus (ILF), Inferior Fronto-Occipital Fasciculus (IFO), Middle Longitudinal Fasciculus (MdLF), Superior Longitudinal Fasciculus I, II and III (SLF), Uncinate Fasciculus (UF) and Vertical Occipital Fasciculus (VOF). Projection fiber bundles: Acoustic Radiation (AR), Anterior Thalamic Radiation (ATR), Corticospinal Tract (CST), Optic Radiation (OR) and Superior Thalamic Radiation (STR). Limbic fiber bundles: Cingulum Bundle: Peri-genual (CBP), Cingulum Bundle: Temporal (CBT), Cingulum Bundle: Dorsal (CBD) and Fornix (FX). Commissural fiber bundles: Anterior Commissure (AC), Forceps Major (FMA) and Forceps Minor (FMI).

Table 1. Demographic information of recovered COVID-19 groups and the control group. *Note: The significant difference is labeled with bold fonts (p<0.05)*

	COVID-19 group (n=51)		Control group (n=31)	P value (MG-NC)	P value (SG-NC)	P value (MG-SG)
	Mild (n=19)	Severe (n=32)				
Age, Mean ± SD	59.37 ± 5.87	63.19 ± 5.37	60.58± 6.42	0.507*	0.085*	**0.022***
Sex, male/female	7/12	16/16	18/13	0.774[#]	0.616[#]	0.398[#]
Education (yrs.)	11.05 ± 3.12	10.84 ±2.67	10.48 ± 3.51	0.789*	0.960*	0.800*
Handedness, right/left	19/0	32/0	31/0	-	-	-
Hematocrit (%)	44.69 ±3.05	44.92 ±3.95	-	-	-	0.835*
Underlying diseases, n (%)						
Hypertension	3(16%)	17(53%)	11(35%)	0.123[#]	0.159[#]	0.008[#]
Diabetes	2(11%)	7(22%)	2(6%)	0.606[#]	0.080[#]	0.304[#]
Coronary heart disease	1(5%)	3(9%)	1(3%)	0.722[#]	0.668[#]	0.597[#]
Symptoms, n (%)			-			
Cough	13(68%)	25(78%)	-			
Fever	16(84%)	27(84%)	-			
Dyspnea	2(11%)	6(19%)	-			
Diarrhea	4(21%)	7(22%)	-			
Headache	1(5%)	5(16%)	-			
Fatigue	5(26%)	15(47%)	-			
Myalgia	2(11%)	6(19%)	-			
Chest tightness	5(26%)	14(43%)	-			
inflammatory markers			-			
CRP	12.07 ± 20.03	91.40 ± 63.14	-	-	-	**0.000***
PCT	0.04 ± 0.02	0.14 ± 0.12	-	-	-	**0.001***
IL-6	5.63 ± 8.87	28.68 ± 43.06	-	-	-	**0.041***

Notes: Data represent mean ± SD; MG = mild type group, NC = normal control, SG = severe type group, CRP = C-reactive protein, PCT = procalcitonin, IL-6 = interleukin-6. Asterisk indicates the significance of two sample t-test; pound sign indicates the significance of Chi-square test.
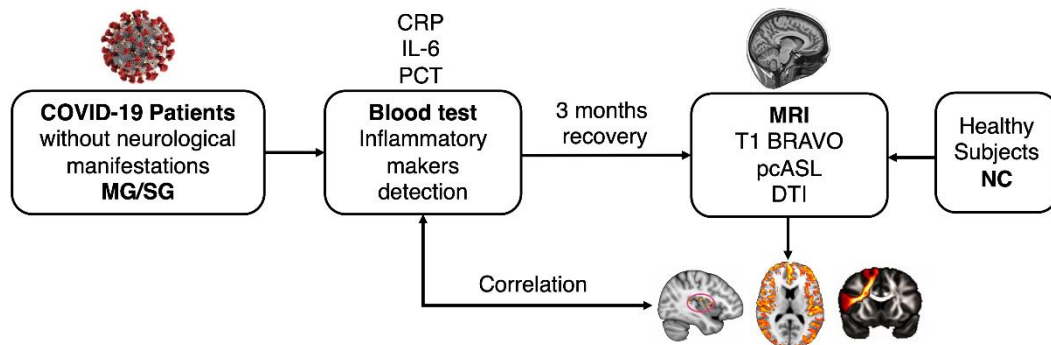
1   **Figures**

2

3   **Figure 1.** Flow diagram of the experimental design. MG = mild group, SG = severe group,
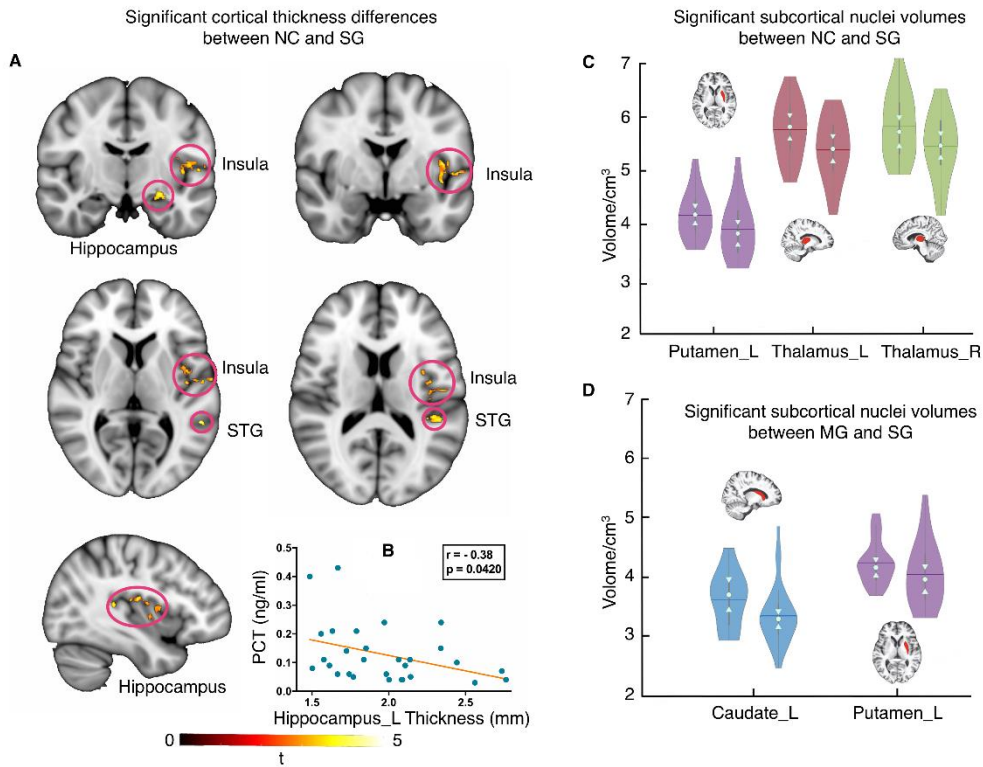
4   CRP = C-reactive protein, IL-6 = interleukin-6, PCT = procalcitonin, MRI = magnetic

5   resonance imaging, BRAVO = brain volume, pcASL = pseudo-continuous arterial spin

6   labeling, DTI = diffusion tensor imaging, NC = normal control.

7

1

2

3 **Figure 2.** Cortical and subcortical morphology analyses of the recovered COVID-19 patients

4 (sample size NC = 31, MG = 19, SG = 32; permutation test, p < 0.05). (A) Significant

5 cortical thickness differences between the NC and SG. (B) Significant negative correlations

6 between the left hippocampus thickness and inflammatory marker PCT values in the SG (r =

7 -0.38, p = 0.0420). Results of subcortical nuclei volume comparisons between the NC and

8 SG (C-Left: NC; Right: SG), MG and SG (D-Left: MG; Right: SG), as exhibited in the violin

9 plot. *Note*: The trunk size shows the probability density of the data at different values, the

10 bigger the trunk, the denser the values appeared at that level. The notch indicates the 25%

11 median and 75% interquartile range. The mean value of the group is shown by solid line. The

12 bigger the standard deviation, the thinner the violin plot. The brain slices of subcortical
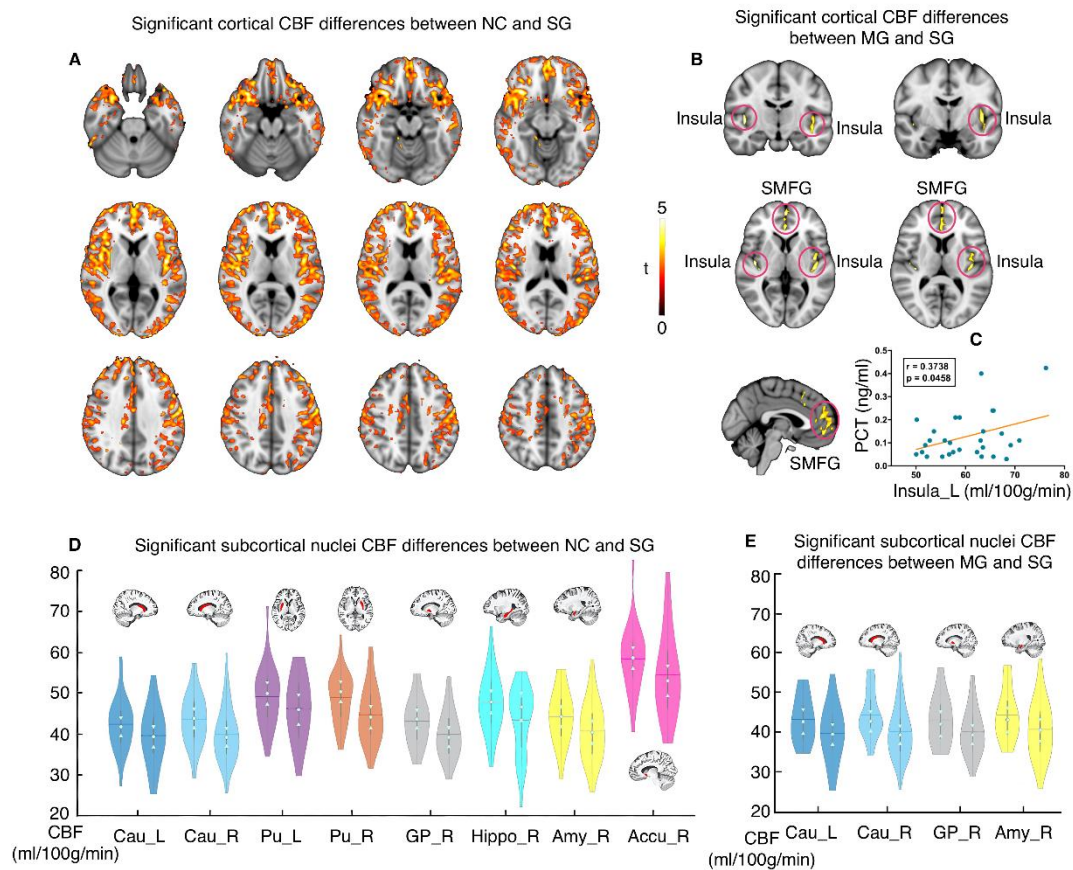
13 nuclei were extracted from a subject. Left violin plots indicate the NC/MG, right violin plots
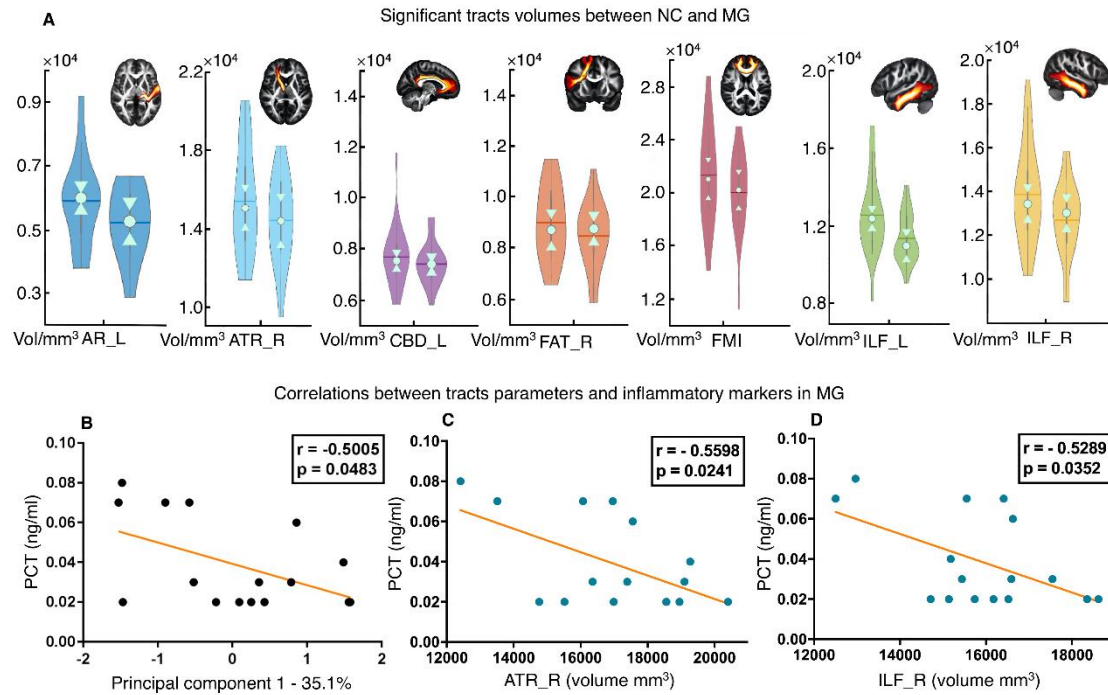
14 indicate the SG. STG: superior temporal gyrus.

15

Figure 3. Significant differences in cortical and subcortical CBF between groups (permutation test, p < 0.05): (A) NC (n=31) and SG (n=32); (B) MG (n=19) and SG (n=32). (C) Significant positive correlation between the left insula CBF and inflammatory marker PCT values in the SG (r = 0.3738, p = 0.0458). Results of the comparisons of the CBF in the subcortical nuclei between groups: (D) NC and SG; (E) MG and SG. Note: SMFG: superior medial frontal gyrus. Left of the brain images is actually the right side of the brain. Accu: accumbens; Amy: amygdala; Cau: caudate; GP: globus pallidus; Hippo: hippocampus; Pu: putamen; L = left; R = right. Left violin plots indicate NC/MG, right violin plots indicate SG.

Figure 4. Significant difference in tracts' volume between the NC (n=31) and MG (n=19) (permutation test, $p < 0.05$). The brai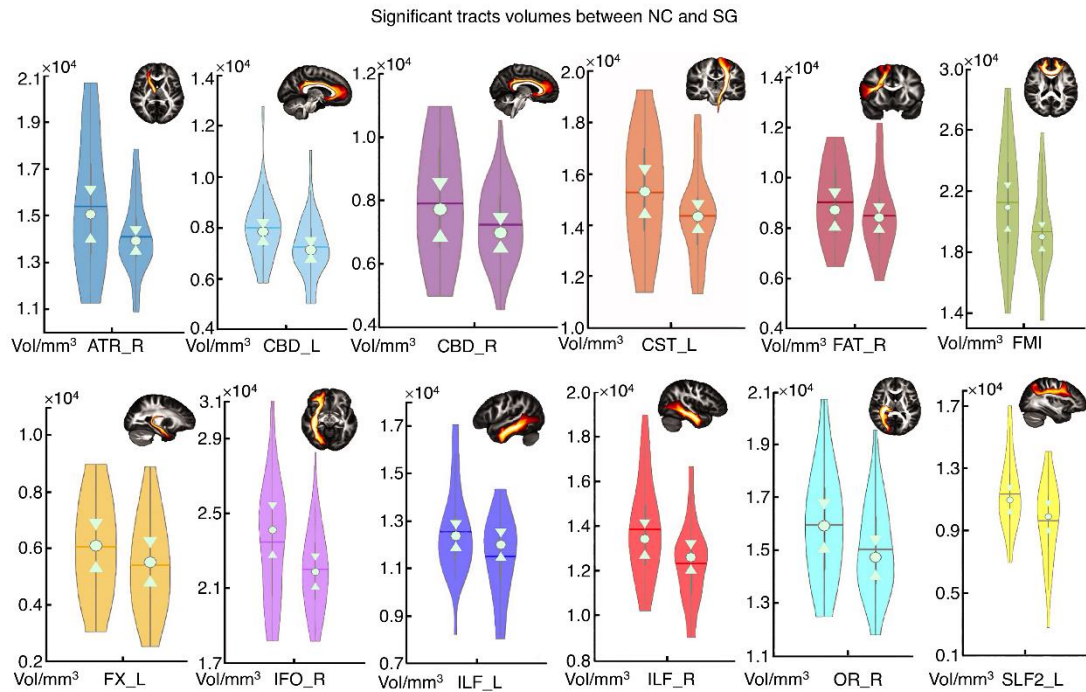n slice of a specific tract from HCP population is displayed in the right corner. For standardization, these tracts were extracted from the HCP population instead of the subjects' specific tracts. The principal component 1 (B), volumes of the right ATR (C) and right ILF (D) showed a significant correlation with the PCT level in the MG ($p < 0.05$). Note: Left violin plots indicate the NC, right violin plots indicate the MG.
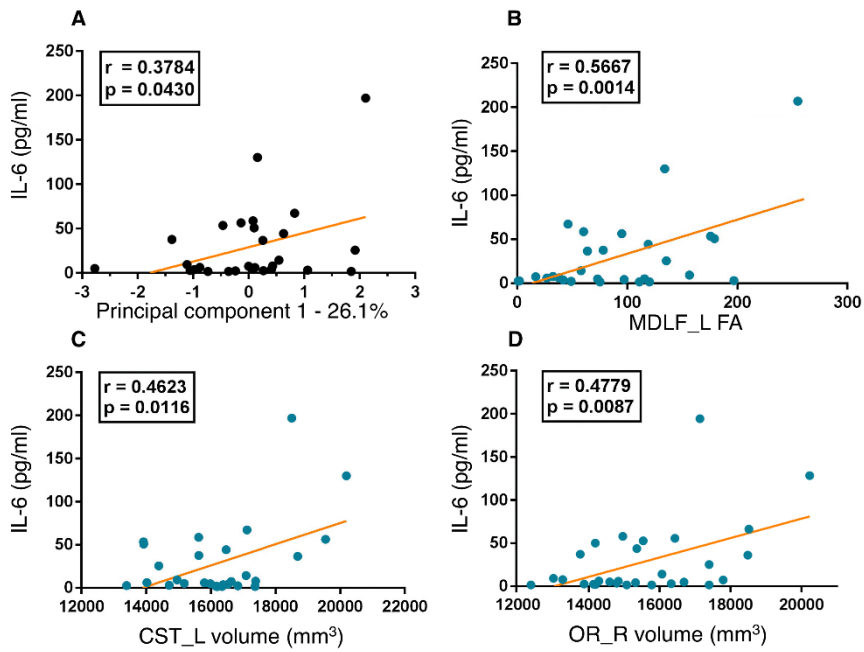
Figure 5. Significant difference of the tracts' volume between the NC (n=31) and the SG (n=32), as shown in violin plots (permutation test, $p < 0.05$). The brain slice of a specific tract from the HCP population is displayed in the right corner. For standardization, these tracts were extracted from the HCP population instead of the subjects' specific tracts. Note: Left violin plots indicate the NC, right violin plots indicate the SG.
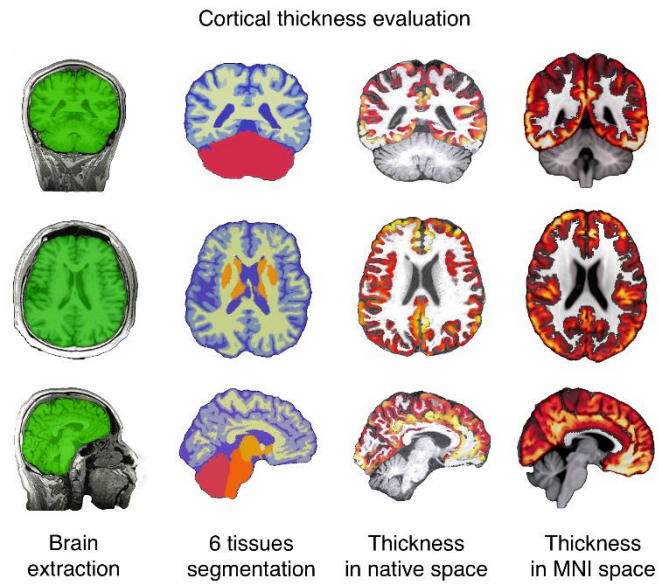
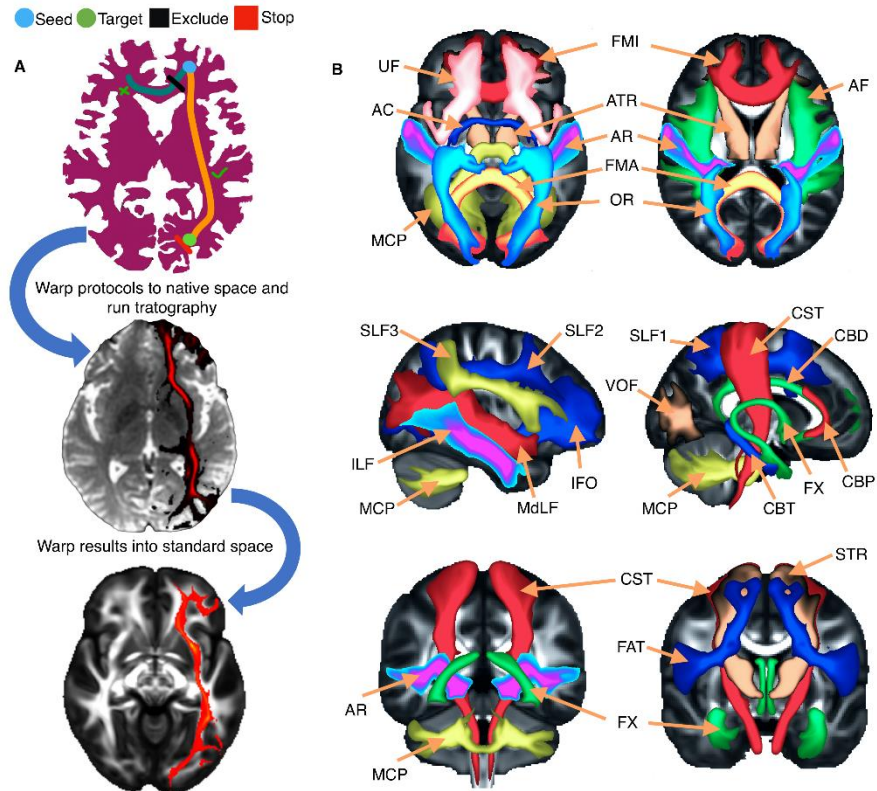Correlations between tracts parameters and inflammatory markers in SG

Figure 6. Correlations between the significantly different tracts and inflammatory markers in the SG (n=32) (p < 0.05). Correlations between the principal component 1(A), FA of left MDLF (B), volume of the left CST(C), volume of the right OR (D) and IL-6 respectively. Note: L = left; R = right.

Cortical thickness evaluation

Brain extraction | 6 tissues segmentation | Thickness in native space | Thickness in MNI space

Figure 7. Workflow of ANTs cortical thickness estimation. ANTs cortical thickness pipeline yielded clear-cut brain extraction and 6 tissues segmentation, as well as nearly perfect estimation of thickness in the native space and accurate warping into the MNI space.

1

2 **Figure 8.** Illustration of the method of XTRACT automated tractography. (A): Diagram of the steps

3 for the XTRACT automated tractography, with an example of the left inferior fronto-occipital

4 fasciculus (IFO). Tractography protocol masks were defined in standard space (FSL_HCP1065

5 FA atlas, derived from the HCP dataset) with seed (start point, blue), exclusion (rejection,

6 black), target (destination, green) and stop (termination, red) masks. The native and standard

7 tractography maps were extracted from a subject from the current sample. (B): Illustration of

8 the projections of the HCP population tract atlases. Association fiber bundles: Arcuate Fascic-

9 ulus (AF), Frontal Aslant Tract (FAT), Inferior Longitudinal Fasciculus (ILF), Inferior Fronto-

10 Occipital Fasciculus (IFO), Middle Longitudinal Fasciculus (MdLF), Superior Longitudinal

11 Fasciculus I, II and III (SLF), Uncinate Fasciculus (UF) and Vertical Occipital Fasciculus

12 (VOF). Projection fiber bundles: Acoustic Radiation (AR), Anterior Thalamic Radiation

13 (ATR), Corticospinal Tract (CST), Optic Radiation (OR) and Superior Thalamic Radiation

14 (STR). Limbic fiber bundles: Cingulum Bundle: Peri-genual (CBP), Cingulum Bundle:

15 Temporal (CBT), Cingulum Bundle: Dorsal (CBD) and Fornix (FX). Commissural fiber

16 bundles: Anterior Commissure (AC), Forceps Major (FMA) and Forceps Minor (FMI).